Journal of Applied Electrochemistry **30**: 1–12, 2000.

Copper deposition on micropatterned electrodes from an industrial acid copper plating bath

S. GOLDBACH[1], B. VAN DEN BOSSCHE[2], T. DAENEN[3], J. DECONINCK[2], F. LAPICQUE[1]*
[1]*Laboratoire des Sciences du Génie Chimique, CNRS-ENSIC-INPL, BP 451, F-54001, Nancy, France;*
[2]*Vrije Universiteit Brussel, VUB-ETEC, Pleinlaan 2, B-1050 Brussel, Belgium;*
[3]*Philips PMF N.V., Glaslaan S17-II-5, NL-5600 Eindhoven, The Netherlands*
*(*author for correspondence, e-mail: lapicque@ensic.u-nancy.fr)*

Received 12 December 1998; accepted in revised form 29 June 1999

Key words: copper deposition, current distributions, microvias, patterned electrodes, simulation

Abstract

Copper was deposited on micropatterned electrodes in a parallel plate reactor (PPR) using an industrial acid copper plating bath, and the deposit thickness distributions were measured. The plating bath contained, besides copper sulfate and sulfuric acid as main components, small amounts of sodium chloride and an organic additive LP-1^{TM}. Copper deposition was carried out under various flow conditions (laminar and turbulent) and applied current densities. Three patterns, each of them consisting of a series of parallel copper microtracks, were manufactured on the electrode surface. The pattern position was chosen to be parallel or perpendicular to the flow direction, corresponding to the two extreme positions for the industrial plating process of patterned electrodes, in casu the round pattern tracks of minicoils. A multi-ion model was used to simulate copper deposition from sulphuric acid solutions, taking into account flow phenomena controlling the mass transfer rate, and the deposition kinetics. The differential equations were solved numerically by use of the multidimensional upwinding method (MDUM). Copper deposition on plane electrodes was investigated and compared to cd distributions obtained from MDUM-simulations. For the case of perpendicular pattern position in laminar flow, the deposit growth in the vias was also modelled and simulated numerically.

List of symbols

a.r.d.	Aspect ratio of copper deposit height on the track top and sidewalls (–)
B_1, B_2	copper deposit thickness on the track sidewalls (μm)
c_b	copper concentration in the bulk (mol m^{-3})
c_s	copper concentration on the electrode surface (mol m^{-3})
d_h	hydraulic diameter $= ZW/(W+Z)$ (m)
d_{meas}	measured thickness of the deposit (μm)
$d_{th,av}$	average theoretical height of the deposit (μm)
D	diffusion coefficient (m^2 s^{-1})
F	Faraday's constant (96 485 A s (equiv)$^{-1}$)
H	copper deposit height on the track top (μm)
i	current density (A m^{-2})
i_{av}	average current density of the cathode (A m^{-2})
i_0	exchange current density (A m^{-2})
i_L	limiting current density (A m^{-2})
$i_{L,av}$	limiting average current density of the cathode (A m^{-2})
k_d	mass transfer coefficient (m s^{-1})
L	cathode length (m)
M_{cu}	molecular weight of copper (63.5 g mol^{-1})
R	Gas constant (8.314 J mol^{-1} K^{-1})
Re	Reynolds number (ud_h/v)
Sc	Schmidt number (v/D_{Cu}^{2+})
Sh	Sherwood number $(k_d d_h/D_{Cu^{2+}})$
Δt	duration of galvanostatic deposition (min)
T	temperature (K)
u	electrical mobility (m^2 mol J^{-1} s^{-1})
$\bar{v}$	average fluid velocity in the channel (m s^{-1})
W	reactor width (m)
Z	channel gap (m)

Greek symbols

α_a	anodic charge transfer coefficient
α_c	cathodic charge transfer coefficient
δ	diffusion layer thickness (m)
δ_h	thickness of the hydrodynamic layer (m)
η	overpotential (V)
κ	electrical conductivity (Ω^{-1} s^{-1})
v	kinematic viscosity (m^2 s^{-1})
v_e	Number of transferred electrons
ρ_{Cu}	density of the copper deposit (8920 kg m^{-3})

1. Introduction

Copper deposition on miniaturized patterns is an important step for the production of printed circuit boards (PCB) and miniaturized motors [1–5]. A thin copper layer is deposited on a polyimide foil by electroless plating. After a photolithographic and etching process, conducting tracks (microvias) are obtained. These must be reinforced by an electrodeposition process to limit the voltage drops, and the warming-up in the circuits of the device, in addition to increase the capacity of the electrical device. Due to the constant trend towards miniaturization, copper must be plated on microstructures with permanently decreasing dimensions. Deposits on these microvias should preferentially grow in vertical direction, to prevent short-circuits between two neighbouring vias. Hence, the formation of mushroom-shaped vias cannot be tolerated. Use of organic additives in the plating bath, for example, LP-1^{TM} [6, 7] for the present investigation, prevents from this type of growth on microstructures.

The advantages of the electroplating step in the production process are high yield, extreme fidelity of pattern transfer and shape replication, easy manufacturing of high aspect ratio structures, rapid processing and low/moderate cost [1].

Numerous investigations were done considering metal deposition in through-mask plating or deposition in through-holes [2–5], [8] but the over-topography plating like the plating on vias with conducting sidewalls was rarely the subject of publications. Only Yung et al. (1989) [9] started with some investigations on copper plating onto vias, and an important difference between via-plating and through-mask plating was observed: the copper distribution in via plating, contrary to through-mask plating, was little influenced by the potential distribution inside the vias. They concluded that mass transport inside small recessed features will be dominated by diffusion instead of convection if the recess is much deeper than it is wide. Their work does not deal with the electrode kinetics, nor with the effect of ion migration phenomena which are included in the numerical calculations, as presented in this work.

Alkire et al. [10, 11] studied mass transfer by diffusion and convection in cavities with various dimensions. Weng and Landau [12] investigated electrode growth of copper patterns on a non-conductive substrate, from an acid copper sulfate bath. Numerical calculations were performed to obtain secondary current density (c.d.) distributions, including the effect of an additive (PEG 400). They considered electroplating on a single pattern, where no cavity geometry was involved for their calculations. On the contrary, pattern growth simulation in this work includes both the effect of the additives (by their influence on the kinetic parameters) and the cavity geometry of the electrode pattern.

In this study the experimental results for copper deposition from a sulfuric acid solution, for different kinds of patterned electrodes in a parallel plate reactor, are presented. This reactor was chosen because of its excellent ability to control the flow conditions above the copper tracks.

A multi-ion model, involving diffusion, migration and convection, is applied to simulate the deposition of copper from sulphuric acid solutions, and solved numerically by use of the multi-dimensional upwinding method (MDUM) [13]. The experimental results for the copper deposit distribution over the length of the electrode will be compared to results for the c.d. distribution obtained from numerical MDUM-simulations. For one kind of patterned electrode, positioned perpendicularly to the flow direction and containing pattern tracks with nonidealised geometry, the final experimental shape of the vias will be compared to the results from the MDUM-simulations, which were to be combined to an electrode growth algorithm.

2. Experimental set-up

2.1. *Parallel plate reactor*

The parallel plate reactor (PPR) was chosen for the presented investigations because of its well-known velocity profiles, provided established fluid flow. The cathode was inserted face downwards to avoid any influence from natural convection [14] for the present case of metal deposition.

The experimental device consisted of a horizontally installed PPR made out of Plexiglas^{TM}, a reservoir for the acidic copper solution, a pump, and a flowmeter. Figure 1 shows a scheme of the flow cell including the flow direction and the electrode positions. The cell was 2 m long and 150 mm broad, and consisted of two halves out of Plexiglas^{TM} bolded together; a spacer also made out of Plexiglas^{TM} was inserted to allow a channel gap at 10 mm near the electrodes. The liquid enters a calming section, where the channel gap is slowly reduced from 60 to 10 mm with a 10° angle, then follows a 570 mm flow development section upstream the electrodes.

The electrodes were fixed with screws in their cell halves: the screws were also used as current leads from the direct current source. The working electrode consisted of a stainless steel or a copper sheet, and was embedded in the upper half of the cell. This cathode had a width of 100 mm and a length of 150 mm. The counter electrode on the opposite wall was made out of copper and was 200 mm long and 150 mm wide. The cathode foils described in the next chapter were fixed on the electrodes with a self-adhesive copper tape (width 10 mm, thickness 100 μm) to ensure the electrical contact between the foils and the electrode substrate.

The solution used for the flow cell experiments was of practical industrial interest: it contained 87 g l^{-1} $CuSO_4 \cdot 5H_2O$ (0.348 M), 2.06 M sulfuric acid, 100 mg l^{-1} sodium chloride and 0.6 vol % LP-1^{TM} additive solution: this last compound is a branch-chained polypropylene ether and was purchased from Blasberg, Germany. High grade chemicals with a purity of about 99% were used.

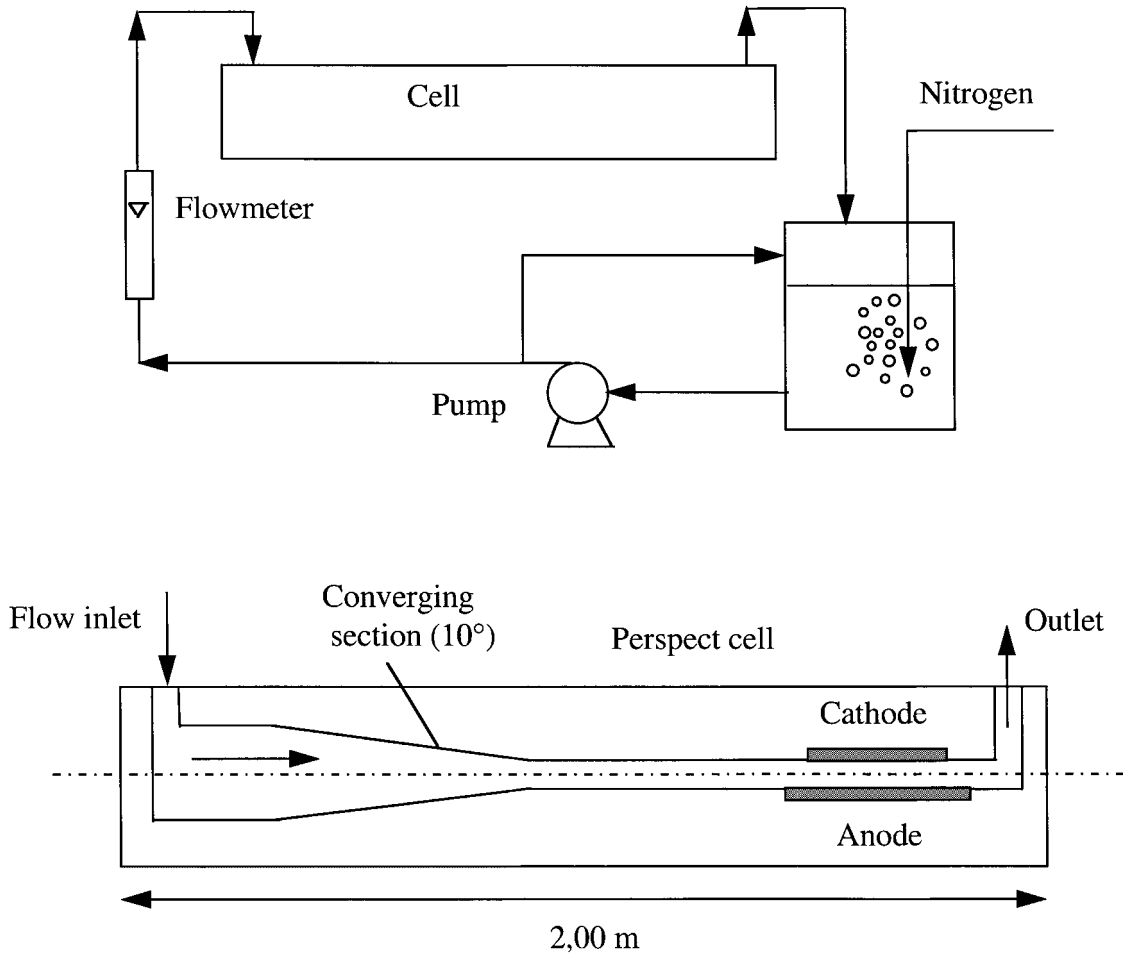

Fig. 1. Scheme of the parallel plate reactor.

2.2. *Cathode material*

The cathode foils consisted of a metal layer (copper or stainless steel, 35 μm) on a polyimide layer of about 30 μm thickness: the copper layer was produced by electroless deposition. The patterns were produced by successive photolithographic and etching processes. The cathode sheets which were selected for the investigations in the flow cell, are shown in Figure 2. Each pattern consisted of a series of ten small copper tracks (80 μm large, 35 μm high) as shown in Figure 2. The gap width between these microvias was chosen to be either 100 μm and 300 μm for both parallel and perpendicular pattern position. The patterns were either perpendicular (Figure 2, on the upper half) or parallel (Figure 2, in the middle) to the electrolyte flow. The etched pattern tracks did not have an ideal rectangular shape, but had inclined side walls due to the lithographic process (Figure 3 and Figure 11). Although this shape differs noticeably from the usual rectangular profiles, it is more relevant to industrial galvanisation processes on small patterns.

Before the deposition in the PPR could be started, the electrode foils were prepared as follows: the copper electrodes were dipped in chromium sulfuric acid for a few seconds, whereas the stainless steel foils were cleaned in 1 M HCl for about 10 min. The stainless steel electrodes were submitted to further treatments: predeposits of a thin nickel layer (0.5 μm) from a Watts bath, and a thin copper or gold layer (1 μm) using a copper or gold cyanide bath, were formed to allow good adhesion of the deposit to be produced from the acid copper sulfate bath.

Galvanostatic deposition runs were carried out for periods ranging from 30 min to about 2 h, depending on flow rate and applied current density, as to obtain deposits with a thickness from 15 to 40 μm. This range of deposit thicknesses allows optimal X-ray measurements. All experiments were carried out at ambient temperature, that is, (21 ± 1) °C.

2.3. *Analysis of the copper deposit on the cathode foils*

Copper deposits on the electrode foils were examined using two different methods: (i) cross-sectionning of the electrodes in the pattern area with a laser beam, insertion of the cross-sectionned foil into a resin, followed by microscope photography of the cross sections to examine the actual morphology of the deposit and deposit thickness; and (ii) thickness measurement by X-ray fluorescence using a Fischerscope model 1500.

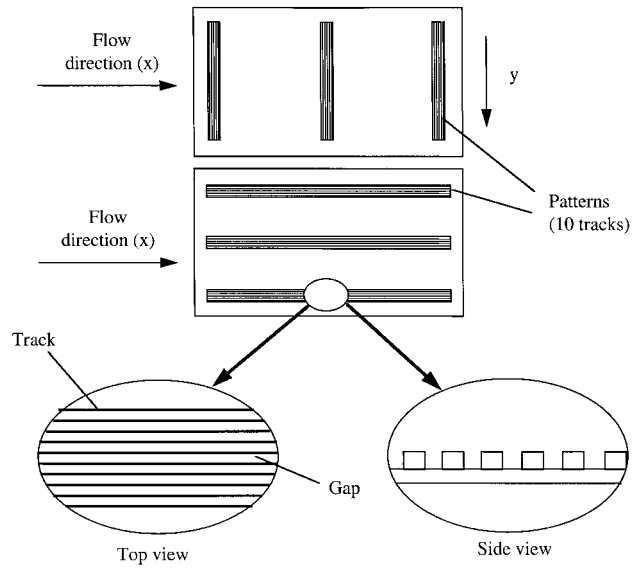

Fig. 2. System of coordinates for the X-ray measurements on plane electrodes and positions of the patterns with respect to the flow direction.

For X-ray measurements of the plane cathode foils without pattern, a system of coordinates was defined as shown in Figure 2. The cross sections were taken in the middle of the electrode ($y = 5$ cm) at the upstream end ($x = 1.1$ cm), in the middle of the foil ($x = 7.5$ cm) and at the downstream end ($x = 13.9$ cm). Additional sections were made near the side wall, at $y = 1.5$ cm and $x = 1.1$ or 13.9 cm.

The most effective method to examine the patterned electrode foils is cross-sectionning of the sample foils at the same positions as the X-ray measurements were taken. Figure 3 illustrates the dimensions of interest of the copper deposit produced on the tracks that were measured from the cross sections.

3. Kinetics of copper deposition and composition of the electrolytic bath

Although copper deposition/dissolution is generally considered to proceed in two steps, the reaction was modelled here as an overall one-step process:

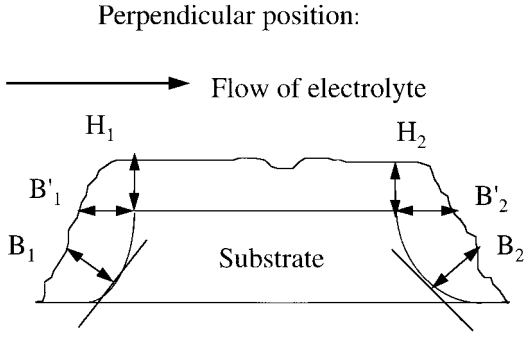

Fig. 3. Significant deposit heights on a cross section of a track.

$$Cu^{2+} + 2e^- \rightarrow Cu$$

The electrochemical data required for the numerical calculations were obtained by potentiodynamic measurements and impedance spectroscopy on a rotating disc electrode (RDE) [15] at room temperature. For the solution mentioned above and used in the production lines, the kinetic and diffusion parameter were obtained by fitting the potential/current density curves with the overall Butler–Volmer law:

$$i = i_0 \left[\exp\left(\alpha_a \frac{F}{RT} \eta \right) - \frac{c_s}{c_b} \exp\left(-\alpha_c \frac{F}{RT} \eta \right) \right] \quad (1)$$

where the surface concentration of copper ions was obtained by

$$i = v_e F k_d (c_b - c_s) \quad (2)$$

the mass transfer coefficient k_d being given by the Levich equation for the RDE.

For the solution of present interest, the exchange current density was determined as $i_0 = 7.4$ A m^{-2}, the charge transfer coefficients were $\alpha_c = 0.48$ and $\alpha_a = 1.05$, and the diffusion coefficient for Cu^{2+}, $D_{Cu^{2+}}$ was measured at 4.22×10^{-10} m^2 s^{-1}. The adsorption and complexing effects of chloride ion and the LP-1™ additive are described quantitatively in a companion paper [15]. However, as far as the numerical modelling in this paper is concerned, the kinetics of the copper deposition was expressed by Relation 1, and the effects of the two additives were taken into account by their influence on the global parameters i_0, α_c and α_a as presented above.

The solution resistance was measured by impedance measurements at the RDE and extrapolation of the spectra at infinite frequency: κ was estimated at 48 Ω^{-1} s^{-1} at ambient temperature [15]. The kinematic viscosity of the solution, v, was determined with an Ubbelohde viscosimeter at 1.43×10^{-6} m^2 s^{-1} [15], corresponding to a Schmidt number of the electrochemical system at 3388.

Generally, concentrations of the various species can be calculated taking into account the dissociation equilibria of copper sulfate and sulfuric acid, together with suitable models for non-ideal behaviour of all species. In the present study, because of the high acid content, sulphate species was neglected and sulfur-containing species were assumed to be in form of hydrogensulphate ion HSO_4^- only. In addition, for the sake of simplicity, copper sulfate was assumed to be fully dissociated into cupric ions and sulfate. Concentrations of introduced copper salt and sulfuric acid with a mass balance on hydrogen led to the initial concentration values of the three ions considered Cu^{2+}, H^+ and HSO_4^- (Table 1).

Table 1. Bulk concentrations of the three species considered in the electrolytic bath and selected values for their diffusion coefficients at ambient temperature

Ion	Concentration/mol m^{-3}	Diffusion coefficient/m^2 s^{-1}
Cu^{2+}	348	4.22×10^{-10}
H^+	1712	5.68×10^{-9}
HSO_4^-	2408	8.12×10^{-10}

4. Description of the numerical simulation

4.1. *Main equations*

In diluted solutions, the flux $\bar{N}_k$ (mol m^{-2} s^{-1}) of each dissolved species k due to diffusion, convection and migration, respectively, was expressed by

$$\bar{N}_k = -D_k \bar{\nabla} c_k + c_k \bar{v} - z_k u_k F c_k \bar{\nabla} U \tag{3}$$

with c_k the molar concentration in mol m^{-3}, z_k the charge, u_k the electrical mobility, U the potential, D_k the diffusion coefficient, $\bar{v}$ the velocity of the forced flow, and F Faraday's constant at 96 487 A s mol^{-1}. For each species k, the local conservation of mass can now be expressed by

$$\frac{\partial c_k}{\partial t} = -\bar{\nabla} \bar{N}_k \tag{4}$$

where $\bar{\nabla} \bar{N}_k$ represents the divergence of the flux vector. The set of equations (4) has to be completed with the local electroneutrality condition:

$$\sum_{k=1}^{I} z_k c_k = 0 \tag{5}$$

in order to obtain a consistent system of equations in which the unknown field variables are the species concentrations and the electrolyte potential. This system of equations will be solved over the reactor domain, under stationary regime, with appropriate boundary conditions. Bulk concentrations of all ions considered are imposed at the entrance of the electrolytic reactor. At insulating boundaries, the flux of all ions must be zero. At the electrodes, the flux of reaction species is directly related to the electrode kinetics as described by Equation 1. The overpotential in this relation represents the difference between the imposed electrode potential V and the local electrolyte potential U adjacent to the electrode, referred to the rest potential E_{rest}:

$$\eta = V - U - E_{rest} \tag{6}$$

The 'multidimensional upwinding method' was presented to solve the dilute solution model in a previous paper [13]. This method is based on a standard 'finite volume' approach for the migration and diffusion contributions, whereas the convection contribution is treated with the 'residual distribution' or 'fluctuation splitting method' [16]. Hence the reactor domain must be discretised into a number of triangles, on which the unknown concentration and potential variables are assumed to have a piecewise linear variation. This approach leaves the values in the triangle corners (nodes) to be determined. Finally, this results in a nonlinear system of equations, to be solved with a Newton–Raphson iterative procedure [17].

4.2. *Diffusion coefficients*

Diffusivities of H^+ and HSO_4^- species were estimated from the measured electrical conductivity κ as follows. In spite of the high electrolyte concentrations, ion mobilities and diffusivities were assumed to be related to κ according to [18]:

$$\kappa = F^2 \sum_{k=1}^{I} z_k^2 u_k c_k \tag{6}$$

$$D_k = RTu_k \tag{7}$$

u_k and D_k appearing in the above relations are overall physical parameters in the considered medium. $D_{Cu^{2+}}$ was determined previously as explained above. The two unknown diffusivities were reduced by the same factor from their values at infinite dilution, D_k^∞, being of 9.310×10^{-9} and 1.331×10^{-9} m^2 s^{-1} at 25 °C for H^+ and HSO_4^-, respectively. The value for the electrical conductivity and the above constraint for ratio D_k/D_k^∞ led to estimates for the diffusion coefficients (Table 1).

4.3. *Calculations for flat electrodes*

4.3.1. *Hydrodynamics and mass transfer rates*

Simulation of the current and potential distributions was conducted for the only case of laminar flows. The electrolyte flow field involved in Equation 3 was calculated in advance and considered as a set of input data for the electrochemical calculations. The usual velocity profile in laminar conditions through a rectangular channel, involves coordinates y and z; however, for the present PPR with a large width/height (W/Z) ratios (15:1 in this case), the axial velocity can be approximated by the simple analytical expression [19]

$$v_x = \bar{v}\left(\frac{z}{Z} - \frac{z^2}{Z^2}\right) \tag{8}$$

where the average velocity $\bar{v}$ was deduced from the liquid flow rate and the cross section of the channel. Modelling was achieved in the two-dimensional system (x–z).

The current density distribution on plane, parallel electrodes has been the subject of numerous investigations. For the limiting current on these electrodes in laminar flow, a dimensionless form of the classical Lévêque [20] equation was used:

$$\frac{i_L}{i_{L,av}} = \frac{2}{3}\left(\frac{L}{x}\right)^{1/3} \text{ with}$$

$$i_{L,av} = 1.85\, v_e Fc \left[\frac{uD^2_{Cu^{2+}}}{d_h L}\right]^{1/3} \quad (9)$$

This equation is valid for channel widths far larger than the electrode gap. The correcting term introduced by Pickett and Stanmore [21] and involving W/Z ratio, reduces the constant in (9) from 1.85 to 1.81 in the present case.

Due to the moderate ratios (L/d_h), the turbulent flow expected for Re over 3000, is not fully established and the current density varies with axial coordinate x; the relation proposed by Stanmore [22]:

$$Sh_{av} = 0.145\, Re^{2/3}\, Sc^{1/3}\left(\frac{d_h}{L}\right)^{0.25} \quad (10a)$$

and valid for (L/d_h) below 7.5, was used for estimation of the average limiting current density, $i_{L,av}$. The local limiting current density was deduced from $i_{L,av}$ after:

$$\frac{i_L}{i_{L,av}} = 0.8\left(\frac{L}{x}\right)^{0.2} \quad (10b)$$

4.3.2. *Mesh generation and calculations*

Quality of the numerical results is to be influenced by the mesh generation in the two-dimensional domain. The grid in the zones adjacent to the electrodes, in particular the cathode, must be refined down to a cell dimension of about 1 μm perpendicularly to the electrode surface, for the sake of accurate description of the local exhaustion of cupric ions by controlling-rate diffusion. Figure 4 shows the grid for a vertical longitudinal cross section of the reactor zone around the electrodes. About 3500 nodes have been used for discretisation of the whole domain The total number of nodes is about 3500.

The CPU time was about 4 min (Silicon Octane workstation), for 10 iterations in the Newton–Raphson iteration method. For near limiting current density conditions (70 to 100% of i_L), a stepwise increase of the applied potential was required to ensure convergence, which increased the CPU-time by a factor up to 3.

4.4. *Calculations in the vias*

The space between two neighbouring tracks is very small and an additional, very fine grid had to be constructed for this most detailed part of the PPR domain. Figure 5 shows the initial shape and mesh used before plating. Cell dimensions were decreased down to 0.5 μm and the number of nodes in and around the vias was about 1500.

For detailed simulations of the vias, the change in electrode shape during the deposition process has to be taken into account. Hence, the total deposition time was divided into a number of time intervals ranging from 1500 down to 500 s. Furthermore, the electrolyte flow in the cavity is laminar, yet complex, and was calculated with a numerical solver for the Navier–Stokes and continuity Equations [23]. A number of repetitive numerical tasks had to be accomplished for calculation of the final shape of the vias after the total plating time, as follows. First, the flow field was calculated and was used for the electrochemical calculations. A vector representation of the flow field at the initial plating stage is given in Figure 6. By use of Faraday's law, the boundary displacement in and around the vias is calculated for the first time interval. New grids are then generated for both the hydrodynamical and electrochemical calculations. The entire loop is repeated several times. Local deposition of copper was generally simulated for lapses of time greater than the experimental durations.

5. Distributions on flat electrodes

5.1. *Method for comparison*

The results of these calculations (i.e., the current density distributions over the cathode) will be compared directly

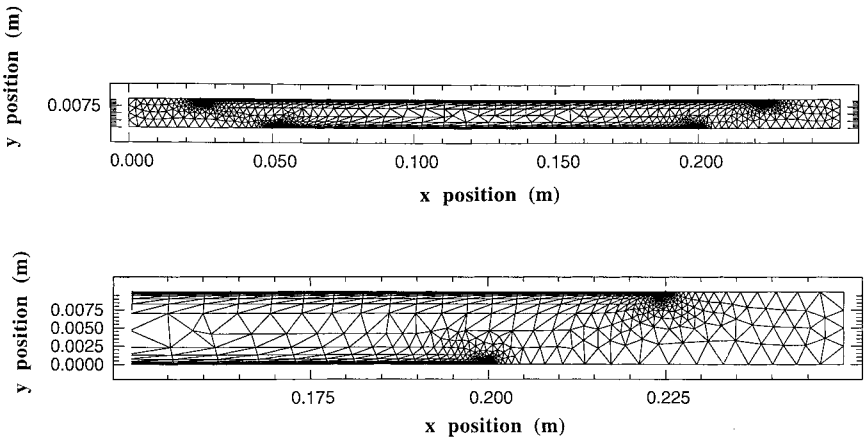

Fig. 4. Triangular mesh for the numerical calculations in the PPR (height and length are not on the same scale).

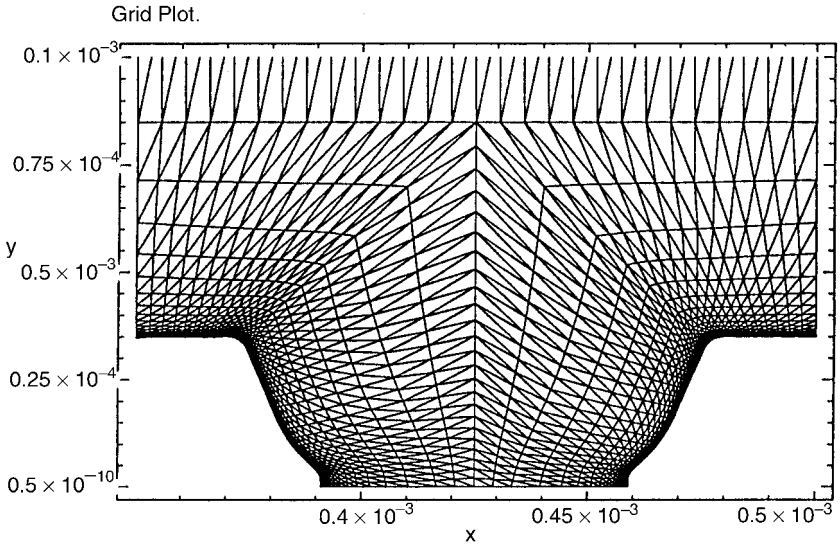

Fig. 5. Triangulation for the numerical calculations in the cavity before deposition.

to experimental measurements of thickness distribution, by use of Faraday's law. The theoretical average thickness of the copper deposit was deduced from Faraday's law assuming a 100% current yield for copper deposition:

$$d_{\mathrm{th,av}} = \frac{i_{\mathrm{av}} \mathrm{M_{Cu}} \Delta t}{\rho_{\mathrm{Cu}} \nu_{\mathrm{e}} F} \tag{11}$$

The average current density was calculated by dividing the applied current by the electroactive surface. The value for the theoretical copper deposit thickness obtained from Equation 11 is averaged over the entire electrode. For direct comparison of the theoretical current density distribution with the measured copper thicknesses on the electrode, the following relationship was deduced:

$$\frac{d_{\mathrm{meas}}}{d_{\mathrm{th,av}}} = \frac{i}{i_{\mathrm{av}}} \tag{12}$$

5.2. *Comparison of experimental and numerical results*

Copper deposition on plane electrodes was carried out under various experimental conditions, that is, flow velocity and imposed current density (Table 2). Replicate of some experiments showed that the error in measuring the local c.d. or deposit thickness could be assessed at a few percent. The experimental c.d. distribution was determined by X-ray measurements of the copper deposit thickness and applying Equation 12. For the case of turbulent flows, c.d. was observed to decrease rapidly in the upstream part of the electrode (data not shown) and to become more uniform in the downstream

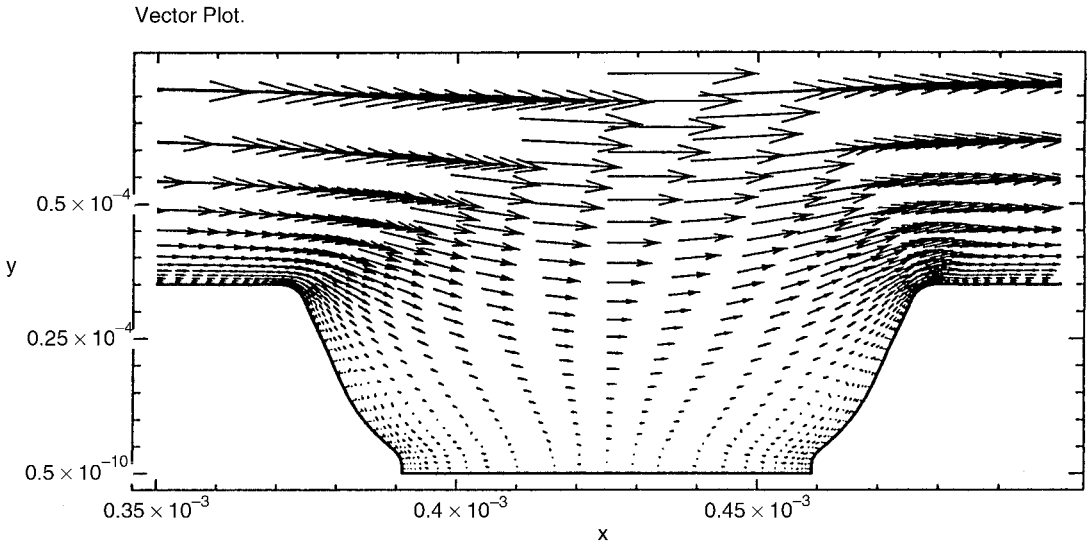

Fig. 6. Electrolyte flow field in the cavity before deposition, $Re = 1160$.

Table 2. Operating conditions for the experiments on nonpatterned electrodes and average values of the deposit thickness (Values for $i_{L,av}$ were calculated using Relations 9 and 10)

Re	i_{av}/A m^{-2}	$i_{L,av}$/A m^{-2}	Fraction of $i_{L,av}$/%	Δt/min	$d_{th,av}$/μm
1160	76	223	34	155	26
1160	127	223	57	90	25
1160	200	223	90	60	26.5
4640	192	553	34	99	41.5
4640	318	553	57	36	25

region. As expected, the decreasing variation with x was favoured by increasing the cell voltage.

The c.d. distributions in laminar flow ($Re = 1160$) modelled by the MDUM-approach are in good agreement with the experimental ones (Figure 7). As expected, the c.d. distribution at the electrode becomes more uniform over the electrode as the applied current is decreased, corresponding to lower fractions of the limiting current. However, near the limiting current (200 A m^{-2}), the current density distribution approaches the theoretical law $i \propto x^{-1/3}$ for laminar flow. For higher or lower laminar fluid velocities in laminar regime, the simulated current density distributions are almost identical to those shown in Figure 7, when compared at the same fraction of the limiting current density.

Scattering of the experimental results at the edges of the cathode was noticed, especially at the downstream end. This was likely due to local disturbance of the flow induced by the self-adhesive copper tape used for fixation of the foil on the support.

6. Results for patterned electrodes

The most important parameter for assessment of the quality of the copper deposit on a track is the aspect ratio of the copper deposit, a.r.d., defined as the deposited metal thickness on the top of the track over that on the track sidewalls as follows:

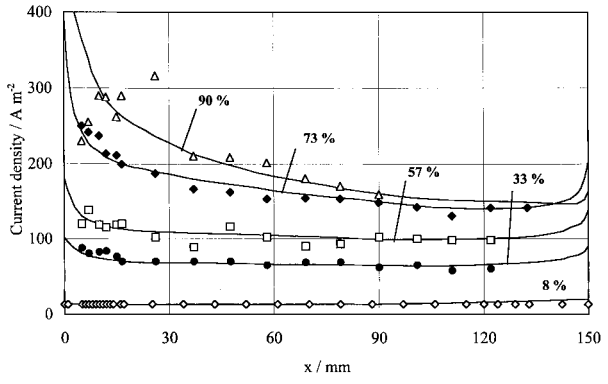

Fig. 7. Cathodic current density distributions in the PPR, $Re = 1160$, $i_{L,av} = 223$ A m^{-2} at various fractions of the overall limiting c.d. Solid lines refer to the model predictions.

$$\text{a.r.d.} = \frac{2H}{B_1 + B_2} \tag{13}$$

where B_1 and B_2 are the deposit thicknesses at 10 μm from the vias bottom, perpendicularly to the initial surface (Figure 3). Values of a.r.d. over unity are preferred to avoid short circuits which might occur from excessive deposit growth on the track sidewalls and at its corners.

6.1. *Experimental results*

The first important result of the experiments is that the copper deposit thickness was not affected by the track number in a series: for parallel or perpendicular position, the deposit thickness on the first track (closer to the upstream edge) is very similar to that on the tenth track of the same series. Therefore the individual values for the deposit thickness were averaged over the examined tracks of one pattern (Table 3).

6.1.1. *Deposit height on the track*

The height of copper deposit on the tracks was compared with that on the copper foil and a few experiments were carried out on non-patterned foils for this purpose. As shown in Figures 8 and 9, the metal thickness on the tracks is as high as those on the flat electrodes. This result shows that the flow is not disrupted by the micropatterns: as a matter of fact, the pattern height (35 μm) can be compared with the thickness of the hydrodynamic layer which is related to the thickness of the diffusion boundary layer:

$$\delta_h = Sc^{1/3}\delta = Sc^{1/3}\frac{k_d}{D_{Cu^{2+}}} \tag{14}$$

Relations 9 and 10 yielded averaged thicknesses δ on the electrode surface, and the results given in Table 4 confirmed that for all cases, the liquid flow could not be disrupted by the 35 μm high tracks.

A zoom-in of the first pattern (i.e., at position $x = 1.1$ cm, $y = 5$ cm) is shown in Figure 10: the deposit of the first tracks is higher than on the last one for a pattern position perpendicular to the flow direction. For this pattern, the diffusion boundary layer varies rapidly with x, and the difference in mass transfer rate between the first and the last track is slightly visible by measurements of the deposit thickness. Data obtained with both X-ray measurements and microscope photographs are presented: the slight difference between the two source of data is discussed in the following Section.

6.1.2. *Distribution of deposit thickness on a track*

For the experiments on copper foils with pattern position to the fluid flow direction, the copper deposit was higher on the top of a rib than on its side walls for 100 μm gaps and high current densities (e.g., 90% of the limiting current density). This effect becomes, as expected, more pronounced on the bottom of the track, and for

Table 3. Aspect ratio values obtained from the microscope photographs of the cross sections at (x, y) locations

Position (x, y)/cm	$2H/(B_1 + B_2)$ a.r.d	$2H/(B'_1 + B'_2)$ a.r.d′.
Parallel position		
Re = 1160, space = 100 μm, $i/i_{L,av}$ = 90%		
(1.1, 5.0)	1.14	1.06
(7.5, 5.0)	1.31	1.19
(13.9, 5.0)	1.33	1.15
(13.9, 1.5)	1.30	1.14
Re = 1160, space = 100 μm, $i/i_{L,av}$ = 33%		
(1.1, 5.0)	1.07	1.06
(7.5, 5.0)	1.02	0.98
(13.9, 5.0)	0.94	1.05
Re = 1160, space = 300 μm, $i/i_{L,av}$ = 33%		
(1.1, 5.0)	0.98	0.98
(7.5, 5.0)	0.97	1.03
(13.9, 5.0)	1.03	1.00
(13.9, 1.5)	0.97	1.07
Re = 4640, space = 100 μm, $i/i_{L,av}$ = 57%		
(1.1, 5.0)	1.16	1.11
(7.5, 5.0)	1.30	1.13
(13.9, 5.0)	1.20	1.12
(1.1, 1.5)	1.20	1.13
Re = 4640, space = 300 μm, $i/i_{L,av}$ = 33%		
(1.1, 5.0)	0.96	0.97
(7.5, 5.0)	0.85	0.90
(13.9, 5.0)	1.01	0.94
(1.1, 1.5)	0.96	1.03
Perpendicular position		
Re = 1160, space = 100 μm, $i/i_{L,av}$ = 57%		
(1.1, 5.0)	1.00	0.98
(7.5, 5.0)	1.11	1.10
(13.9, 5.0)	1.03	1.03
(1.1, 8.5)	1.07	1.02
Re = 1160, space = 300 μm, $i/i_{L,av}$ = 33%		
(1.1, 5.0)	0.91	0.91
(7.5, 5.0)	1.00	1.00
(13.9, 5.0)	0.94	1.09
(13.9, 1.5)	1.06	1.08
Re = 4640, space = 100 μm, $i/i_{L,av}$ = 57%		
(1.1, 5.0)	1.03	1.00
(7.5, 5.0)	0.97	0.99
(13.9, 5.0)	1.10	0.93
(1.1, 1.5)	1.03	1.01
Re = 4640, space = 300 μm, $i/i_{L,av}$ = 33%		
(1.1, 5.0)	0.94	1.08
(7.5, 5.0)	0.95	1.05
(13.9, 5.0)	0.97	1.00
(1.1, 1.5)	1.10	1.11

instance, a.r.d. values were measured at 1.30 and 1.15 at distances from the foil of 12.5 μm and 35.0 μm, respectively. For small current densities, the copper deposit thickness on the track top was as large as on the track walls: the deposition was under kinetic control and was not influenced by the gap width between the microvias. For turbulent flows, the distributions were quite comparable with those in laminar flow (Table 3).

For the pattern position perpendicular to the fluid flow direction, and for mass transfer controlled deposition, the positions on the cathode exerted a large influence on the aspect ratio a.r.d.: on the upstream end, the copper deposit on the copper track top can be expected to be similar to that on the track walls because

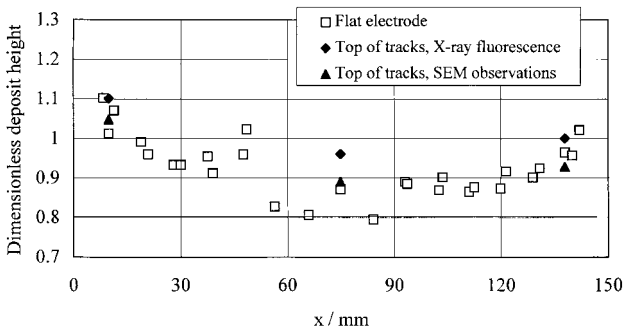

Fig. 8. Dimensionless copper deposit height on the tracks and over the entire electrode; $Re = 1160$, $i = 127$ A m^{-2} ($i/i_{L,av} = 57\%$).

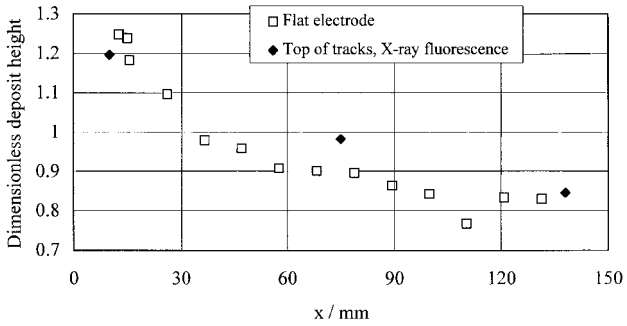

Fig. 9. Dimensionless copper deposit height on the tracks and over the entire electrode; $Re = 1160$, $i = 200$ A m^{-2} ($i/i_{L,av} = 90\%$).

of the small dimensions of the developing diffusion layer. This effect may ensure efficient transfer of fresh fluid into the pattern gaps which results in an even copper deposit growth over the whole pattern track (a.r.d. = 1.00). In the centre and the downstream edge of the electrode, the diffusion layer is sufficiently thick to control the deposition: fresh copper solution reaches preferentially the track top, yielding thicker deposits on top (a.r.d. = 1.05–1.10). As for parallel patterns, there was no difference of the copper deposit thickness on the top and the sidewalls for parallel position as long as copper was deposited under kinetic control. On the contrary, for higher fractions of the limiting current, the influence of diffusion and convection became stronger and one might expect the deposition to be favoured on the top in comparison to the gap walls, as for patterns in parallel position to the fluid flow direction.

For the perpendicular patterns, dimensionless thicknesses B_1/B_2 and B'_1/B'_2 were also considered (Table 5) for comparison of the deposit thickness on the facing sidewall with that on the rear wall of a track. No significant influence of any operating parameter could be detected from the measurements done; B_1/B_2, and

Table 4. Theoretical data for mass transfer rates from Relations 9 and 10 and estimates for thicknesses δ and δ_h

Re	Sh	k_d/m s^{-1}	δ/μm	δ_h/mm
1160	146	3.28×10^{-6}	122	1.93
4640	360	8.11×10^{-6}	52	0.78

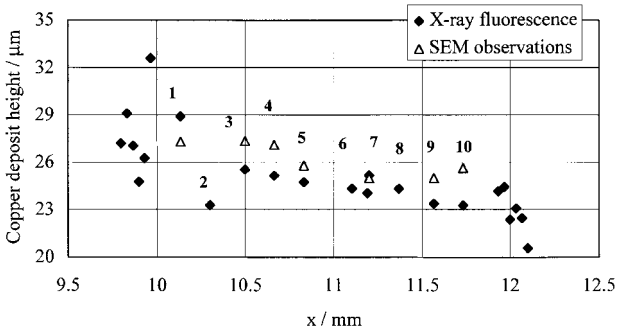

Fig. 10. Zoom-in on the copper deposit height of the upstream pattern ($x = 1.1$ cm and $y = 5.0$ cm), for patterns perpendicular to the flow; $Re = 1160$, $i = 127$ A m^{-2} ($i/i_{L,av} = 57\%$), gap width 100 μm. The figures given refer to the track number.

B'_1/B'_2 varied in the range of 0.86 and 1.18, so B_1, and B_2 were considered comparable.

The pattern ribs were also analysed by X-ray fluorescence measurements. These measurements however being in fair agreement with the cross-section results, were not as accurate as the cross-section analyses (data not shown). Reliability of the measurements was affected by the measurement area of the X-ray apparatus (60×60 μm^2); the dimension of this area is comparable with the width of the tracks, and the values obtained using this technique may be erroneous if the X-ray beam is not perfectly focused on the top of the track. To overcome this problem, measurements were carried out moving the beam focus by successive steps perpendicularly to the pattern tracks, and erratic data corresponding to side signals emitted by the walls were discarded. Measurement error was assessed by the standard deviation to the deposit thickness from six measurements at the same position on the cathode foil. The error of the X-ray measurements was near 3.5% for a copper thickness about 25 μm and about 1.4% for a copper thickness about 10 μm.

6.2. *Comparison of the experimental and numerical results*

Numerical calculations were performed for the case of perpendicular pattern position with a gap width between the microvias of about 100 μm in laminar flow, for $Re = 1160$. A moderate average current density of 127 A m^{-2} was applied to the cathode foil (57% of the overall limiting current). To obtain the average copper deposit height of 25 μm, the deposition was carried out for 90 min. Figure 11 shows the SEM view of the cross section of a microvia in the centre of the electrode ($x = 7.5$ cm, $y = 5$ cm): the deposit growth in vertical direction on the top of the microvia increases with increasing deposition time while the cavities between the microvias become smaller. The simulated growth for the same conditions is presented in Figure 12. Values for a.r.d. were calculated for the upstream and downstream track sides separately, corresponding to thickness B_1 and B_2, respectively. The predicted values for a deposition time of 90 min were compared to the measured thickness in Table 6, and an excellent agreement between the experimental and calculated results of the copper deposit growth can be observed.

Moreover, on the one hand, simulation of the deposition procedure results shows that the potential variations in the vias are below 1 mV, and the influence of migration is negligible in this case. On the other hand, cupric ion depletion at the bottom of the vias increases from about 7% when starting the run, to 25% after 90 min, and exceeds 50% after 120 min: as on the macroscopic surface of the electrode, the deposition in the microstructures is partly controlled by diffusion for the considered c.d.

Table 5. Aspect ratios on the upstream (1) and downstream (2) sidewalls on various tracks in perpendicular configuration (track number increases with x); $Re = 1160$, $i_{L,av} = 223$ A m^{-2}

Position (x, y)/cm	Track number	H/B_1	H/B_2	B_1/B_2	H/B'_1	H/B'_2	B'_1/B'_2
$i/i_{L,av} = 57\%$, 100 μm gap							
(1.1, 5.0)	1	0.94	1.10	0.85	1.00	1.00	1.00
	4	1.06	1.03	1.03	1.06	0.97	1.09
	7	0.89	0.97	0.92	0.89	0.97	0.92
(7.5, 5.0)	1	1.08	1.08	1.00	1.18	1.00	1.18
	6	1.17	1.11	1.06	1.17	1.05	1.11
(13.9, 5.0)	1	1.04	1.04	1.00	1.04	1.04	1.00
	3	1.03	1.07	0.96	0.97	0.91	1.07
	6	1.03	1.03	1.00	0.97	1.03	0.94
(1.1, 8.5)	1	1.16	1.13	1.03	1.06	1.00	1.06
	5	1.06	1.00	1.06	1.03	1.00	1.03
	9	1.03	1.03	1.00	1.07	0.94	1.14
$i/i_{L,av} = 33\%$, 300 μm gap							
(13.9, 5.0)	1	1.09	1.13	0.96	1.15	1.24	0.93
	5	0.94	1.09	0.86	0.88	1.07	0.82
(13.9, 1.5)	1	1.13	1.03	1.00	1.13	1.17	0.96
	6	1.00	0.97	1.03	1.11	0.97	1.14
	10	1.06	1.06	1.00	1.03	1.06	0.97

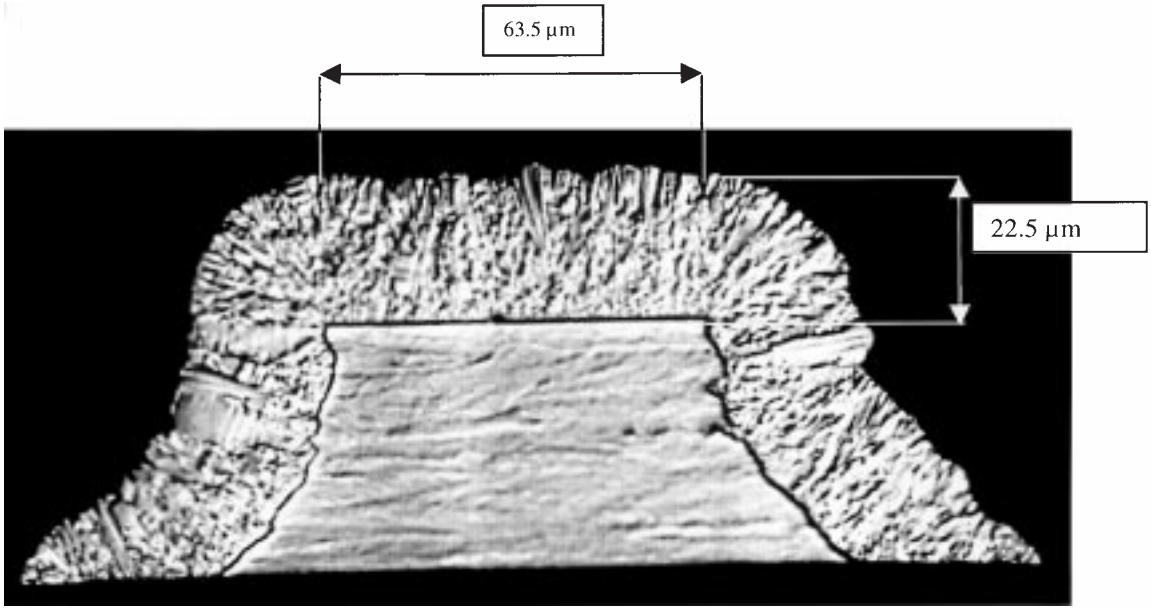

Fig. 11. SEM photograph of a sectioned microvia located in the centre of the electrode ($x = 7.5$ cm, $y = 5.0$ cm). Copper deposit produced for 90 min at 127 A m^{-2} ($i/i_{L,av} = 57\%$), $Re = 1160$.

It can be observed that the electrolyte solution, including small amounts of sodium chloride and the organic additive LP-1^{TM}, allows a correction of the pattern shape since the side walls tend towards a more rectangular shape of the gap as the deposition progresses (Figure 13). Though since the initial etched shape was severely nonideal, the 'corrective effect' of deposition carried out with this electrolytic bath is only partial, and short circuits between two neighbouring tracks may occur after very long deposition times as suggested by the profiles in Figure 12.

7. Conclusion

The work presented aimed at observing copper growth on small-scale patterns, and furthermore validating the theoretical model and the numerical MDUM solution method for accurate simulation of copper deposition on minaturised patterns, from an industrial copper bath.

Taking into account the kinetics of the copper deposition previously determined [15], and the operating conditions in the PPR, namely the applied current density and the fluid flow velocity, the model allows

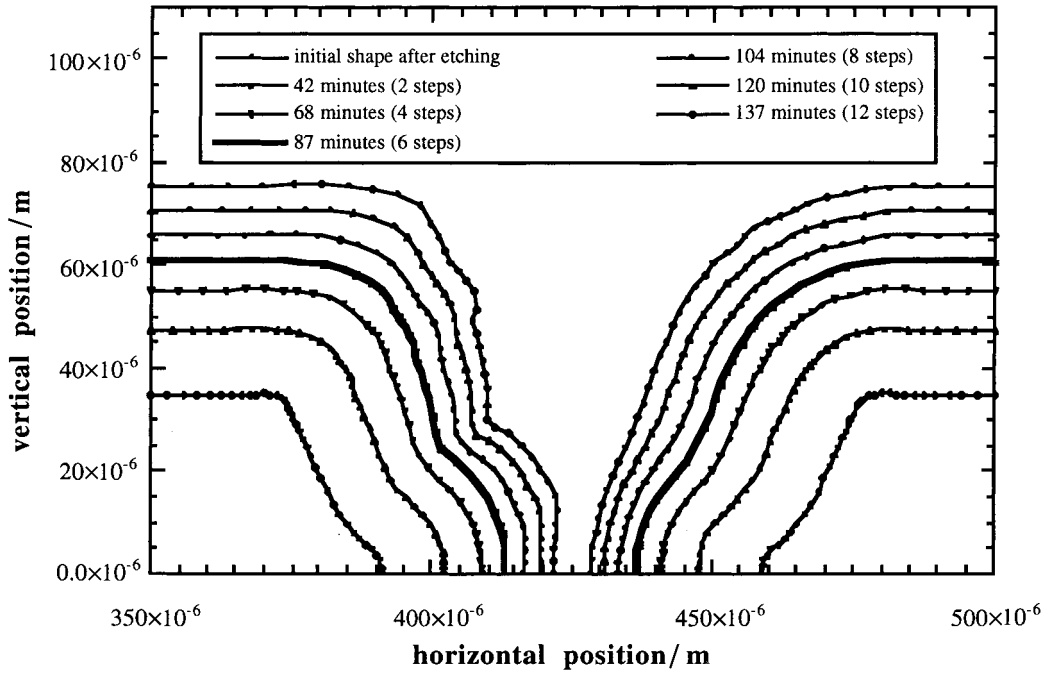

Fig. 12. Pattern growth calculated by the MDUM-method; $Re = 1160$, $i = 127$ A m^{-2} ($i/i_{L,av} = 57\%$).

Table 6. Aspect ratios on the upstream and downstream sidewalls of the tracks: comparison of predicted values with experimental data. Perpendicular position, $Re = 1160$, gap width 100 μm and $i = 127$ A m^{-2} ($i/i_{L,av} = 57\%$)

H/B simulated at step 6, i.e. after 87.5 min	H/B simulated at step 4, i.e. after 68 min	H/B exp. after 90 min upstream/downstream
1.15 (upstream) 1.09 (downstream)	1.12 (upstream) 1.08 (downstream)	1.13/1.04 (track 1) 1.08/1.05 (track 4) 1.17/1.08 (track 6) 1.14/1.10 (track 10) (Average at 1.13/1.08)

predictions of the distribution of copper thickness on the tracks of miniaturised circuits. Copper deposition on plane parallel electrodes was simulated for various fractions of the limiting current and the results were shown to be in excellent agreement with the experimental data. Modelling of the copper deposit growth on a single track yields thickness distributions in the gap very close to the experimentally obtained results.

The copper deposit thickness is nearly the same on flat electrodes as on patterned surfaces, and as expected, the micropatterns do not disrupt the flow over the electrode.

For low to moderate current densities relative to the limiting c.d., the effect of the operating conditions on the thickness distribution on the microtracks is of minor extent: the deposit is as thick on the sidewalls as on the top of the track. Nevertheless, the deposit quality is influenced by the applied c.d.: the dendritic growth of the copper deposit overwhelms for high c.d.'s in turbulent flow. From a more practical point of view for the industrial application of the deposition process, one may expect a faster copper deposit growth in vertical direction (on the top of a micro-via) for a deposition process controlled by diffusion and convection.

Acknowledgements

The work was sponsored by the European Union in the frame of the Brite-Euram III programme BRPR-CT95-0008, and by the Flemish government (IWT, B. Van den Bossche).

References

1. S. Mehdizadeh, J.O. Dukovic, P.C. Andricacos, L.T. Romankiw and H.Y. Cheh, *J. Electrochem. Soc.* **139** (1992) 78.
2. S. Mehdizadeh, J.O. Dukovic, P.C. Andricacos, L.T. Romankiw and H.Y. Cheh, *J. Electrochem. Soc.* **140** (1993) 3497.
3. A.F. Bernhardt, A.T. Bargknecht, R.J. Contolini, V. Malba, S.T. Mayer, N.F. Raley and D.B. Tuckerman, *Appl. Surf. Sci.* **46** (1990) 121.
4. T. Kessler and R. Alkire, *J. Electrochem. Soc.* **123** (1976) 990.
5. E.K. Yung, L.T. Romankiw and R.C. Alkire, *J. Electrochem. Soc.* **136** (1989) 756.
6. H. Iwan, M. Schmitz and H.K. Werner, 'Saures galvanisches Kupferbad und Verfahren zu seiner Herstellung', *European patent*, *Blasberg*, *Nr.84 111402.8* (25 Sept. 1984 Int. Cl. C 25 D 3/38).
7. E. Knaak, J. Hupe and W. Metzger, 'A new acid copper solution for one-compound sulfur-free additive for high-tech application', Blasberg Mittelung 357 (1989).
8. E. Hume, W.M. Deen and R.A. Brown, *J. Electrochem. Soc.* **131** (1984) 1251.
9. E.K. Yung and L.T. Romankiw, *J. Electrochem. Soc.* **136** (1989) 206.
10. R.C. Alkire and D.B. Reiser, *J. Electrochem. Soc.* **131** (1984) 2795.
11. R.C. Alkire, H. Deligianni and J.B. Ju, *J. Electrochem. Soc.* **137** (1990) 818.
12. D. Weng and U. Landau, *J. Electrochem. Soc.* **142** (1995) 2598.
13. L. Bortels, B. Van den Bossche and J. Deconinck, *J. Electroanal. Chem.* **404** (1996) 15.
14. C.W. Tobias and R.G. Hickman, *Z. Phys. Chem.* Bd **229**, H. 3/4.
15. S. Goldbach, W. Messing, T. Daenen and F. Lapicque, *Electrochim. Acta* **44** (1998) 323.
16. R. Struijs, H. Deconinck and P.L. Roe, VKI LS 1990-04, 'Comp. Fluid Dynamics' (1990).
17. L. Bortels, PhD thesis, Vrije Universiteit Brussel, Brussels (1996).
18. J. Newman, 'Electrochemical Systems' (Prentice Hall, NJ, 1991).
19. D.J. Pickett, 'Electrochemical Reactor Design' (Elsevier, New York, 1977).
20. M.A. Lévêque., *Annales des Mines*, *Memoires*, ser. 12,13 (1928) 210.
21. D.J. Pickett and K.L. Ong, *Electrochim. Acta* **19** (1974) 875.
22. B.R. Stanmore, MSc thesis, University of Manchester (1970).
23. T. De Mulder, PhD dissertation, KU Leuven (1997).